Vibrational analysis of phase III of poly (vinylidene fluoride)

M. A. Bachmann and J. L. Koenig

Citation: The Journal of Chemical Physics **74**, 5896 (1981); doi: 10.1063/1.440908
View online: http://dx.doi.org/10.1063/1.440908
View Table of Contents: http://scitation.aip.org/content/aip/journal/jcp/74/10?ver=pdfcov
Published by the AIP Publishing

Vibrational analysis of phase III of poly (vinylidene fluoride)

M. A. Bachmann

Department of Physics, Case Western Reserve University, Cleveland, Ohio 44106

J. L. Koenig

Department of Macromolecular Science, Case Western Reserve University, Cleveland, Ohio 44106
(Received 18 December 1980; accepted 4 February 1981)

Normal coordinate calculations have been performed for an isolated chain having the conformation of phase III of poly (vinylidene fluoride). A valence force field, which was refined from phase I and phase II data, was transferred to the phase III chain calculation. The agreement between the calculated and observed spectra of phase III was good, and approximate normal mode assignments for most of the phase III bands were made. The geometric dependence of calculated frequencies and potential energy distribution for the phase I and phase II chain conformations were also studied.

INTRODUCTION

Poly(vinylidene fluoride) (PVF_2), exists in at least four different crystalline phases. Phase I (β phase) has a planar (all *trans*) zigzag chain conformation with the space group being $Cm2m$.[1,2] Phase II (α phase) has a chain conformation which is approximately $TGTG'$ (*trans–gauche–trans*–minus *gauche*) with the chains packing in a nonpolar unit cell of space group $P2cm$.[2–4] Phase IV (α_p phase, δ phase) possesses essentially the same chain conformation as phase II; however, the chains pack in a polar unit cell of space group $P2_1cn$.[5–8] Phase III (γ phase) has been found to have a chain conformation which is approximately $TTTGTTTG'$ with the space group being $C2cm$.[9,10] Figure 1 shows the three types of chain conformations involved in the crystalline phases of PVF_2.

A number of infrared and Raman studies have been done on the various phases of PVF_2.[11–17] Normal coordinate calculations have been performed on phases I and II using both valence force fields[11,12,17] and a Urey–Bradley force field.[14] Several works have reported on the infrared[15,16] and Raman[12] spectra of phase III. In this work we will present the results of a normal coordinate calculation performed on an isolated chain having the conformation of phase III using the valence force field of Boerio and Koenig.[11] The geometric sensitivity of the calculated frequencies and the potential energy distribution (PED) of phases I, II, and III are also discussed.

EXPERIMENTAL

All three phases of PVF_2 studied in this work (I, II, and III) were prepared from Pennwalt Kynar 460 pellets ($\bar{M}_w = 451\,000$, $\bar{M}_n = 16\,000$). Solutions were prepared by dissolving the pellets in *N,N*–dimethylacetamide (DMA).

The oriented phase I samples were prepared from unoriented phase II films by uniaxially drawing the films at room temperature. The unoriented phase II films were produced by melting films (temperatures in excess of 200 °C) cast at 60 °C from DMA and then quenching the films at room temperature. The polarized infrared absorbance spectrum of phase I is shown in Fig. 2. The oriented phase II samples were prepared from unoriented phase II films by uniaxially drawing the films at 150 °C. The polarized infrared absorbance spectrum of phase II is shown in Fig. 3. Unoriented phase III films were produced by casting films at 60 °C from DMA. The oriented phase III samples were prepared from unoriented phase III films by uniaxially drawing at 174 °C. The polarized infrared absorbance spectrum of phase III is shown in Fig. 4.

The spectra were taken using a Digilab model FTS-14 Fourier transform spectrophotometer. The polarizer was a AgCl plate stack set at the Brewster angle. No correction for imperfect polarization by the polarizer was made.

CALCULATIONS

The normal coordinate calculations were performed on a Digital VAX-11 computer using a program described by Boerio[18] and Hannon.[19] The program requires as input the Cartesian coordinates, atomic masses, internal coordinate definitions, symmetry coordinates, and a set of force constants. The internal coordinate definitions are shown in Fig. 5. External symmetry coordinates were generated from these internal coordinates. The use of external symmetry coordinates yields the displacement coordinates (eigenvectors) in terms of Cartesian coordinates, which simplifies the assignment of the modes calculated.

The chain conformation of phase III is known[9,10] to be approximately $TTTGTTTG'$. The actual configurational parameters for bond angles, bond lengths, and internal rotation angles are given by Weinhold *et al.*[10] The geometric features pertinent to the normal coordinate calculations of phase III presented in this work will be summarized. The $TTTGTTTG'$ conformation can be divided into two domains.[16] There are segments with TTT internal rotation angles which are locally similar to the all-*trans* phase I conformation, and there are segments with TGT or $TG'T$ internal rotation angles which are locally similar to the $TGTG'$ phase II conformation. It will be assumed that the angular parameters describing the conformation of the phase III chain are similar. This is found to be the case for the chain conformation presented by Weinhold *et al.*[10] The TTT seg-

 0021-9606/81/105896-15$01.00

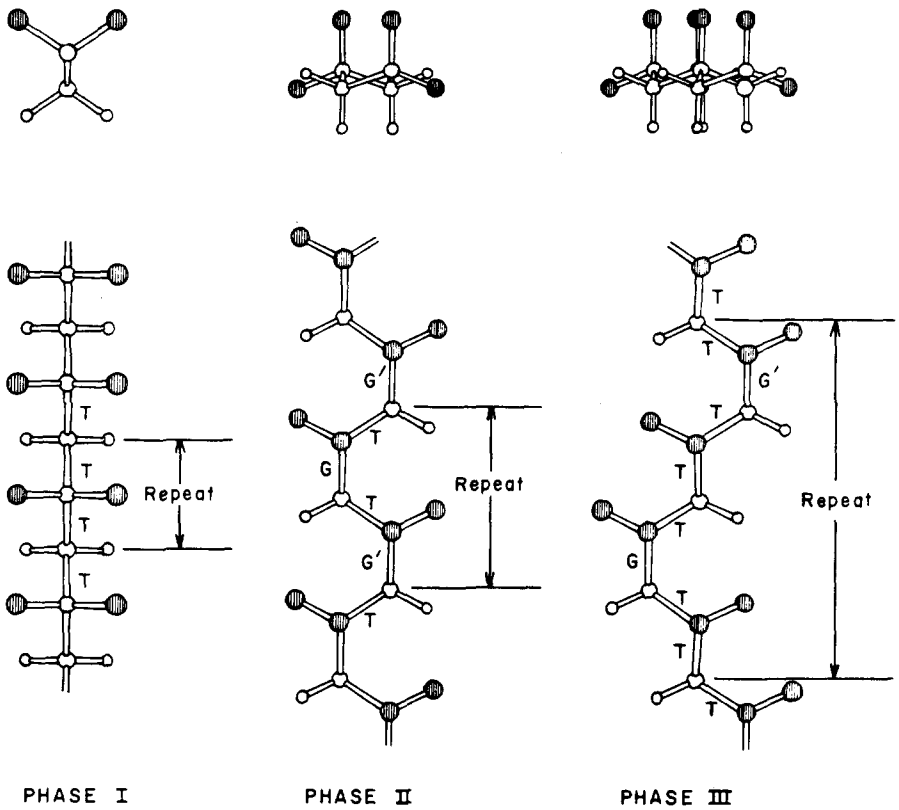

FIG. 1. The three types of chain conformations of poly(vinylidene fluoride). From left to right; all-*trans* phase I, *TGTG'* phase II (and phase IV), *TTTGTTTG'* phase III.

ments have CCC bond angles of 118.0° and 117.3°. The CF_2 bond angles are 104.1° while the CH_2 bond angles are 105.7° in the *TTT* segments. The *trans* internal rotation angles were not 180° but, instead, 170.4° and 171.5°. The *TGT* and *TG'T* segments have CCC bond angles of 114.7° and 115.0°, respectively. The CF_2 bond angles are 102.2°, while the CH_2 bond angles are 103.5° in the *TGT* and *TG'T* segments. The *gauche* internal rotation angle was found to be 51.5°. The error in the values of the bond angles was estimated[10] to be ±1° and possibly larger for the internal rotation angles. Within these error bounds it is seen that the CCC bond angles for the *TTT* segments can be taken as the average value of 117.6°, and for the *TGT* segments as the average value of 114.9°. The CH_2 and CF_2 bond angles for the *TTT* segments can be taken as the average value of 105°, and for the *TGT* segments as the average value of 103°.

All of the normal coordinate calculations presented in this work are zero-order calculations in that the valence force field of Boerio and Koenig[11] is used without any further refinement to improve the fit between observed and calculated frequencies. The force field[11] is given in Table I. Boerio and Koenig[11] obtained this valence force field by transferring force constants from polyethylene[20] and polytetrafluoroethylene,[21] and refining these force constants with the damped least squares method[21,11] using both phase I and phase II data. For the force constant refinement,[11] the CH bond length was

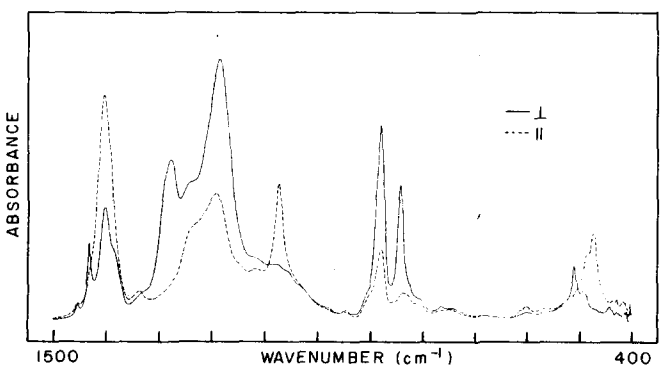

FIG. 2. Polarized infrared absorbance spectrum of phase I of poly(vinylidene fluoride): (—) electric vector perpendicular to the drawing direction; (- - -) electric vector parallel to the drawing direction.

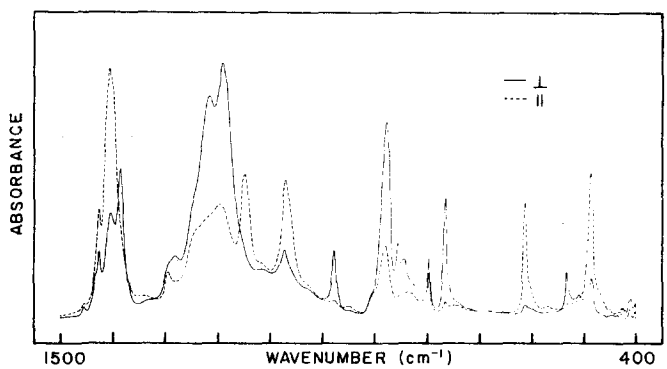

FIG. 3. Polarized infrared absorbance spectrum of phase II of poly(vinylidene fluoride): (—) electric vector perpendicular to the drawing direction; (- - -) electric vector parallel to the drawing direction.

taken as 0.109 nm, the CF bond length as 0.134 nm, and the CC bond length as 0.154 nm. The CH_2 and CF_2 bond angles were assumed to be tetrahedral for both the phase I and phase II chains. The CCC bond angles used in the all-*trans* phase I chain were 113.1°. The CCC bond angles used in the $TGTG'$ ($G=60°$) phase II chain were 115.6°. The interaction force constants which involved next-nearest-neighbor interactions or greater were assumed to be zero. This assumption was necessary because there is not enough data to determine the force constants for these presumably weaker interactions. Because of the conformational similarity of phase III to phases I and II, we assume that the valence force field of Boerio and Koenig[11] can be transferred to the phase III chain. We would expect to be able to identify bands which are characteristic of the TTT phase I regions and TGT and $TG'T$ phase II regions and make approximate normal mode assignments for most of the phase III bands. However, since the force field is limited to nearest-neighbor interactions, we would not expect to be able to make structural predictions for the eight carbon repeat unit of phase III.

Two sets of calculations were done for an isolated phase III chain, with each calculation differing only in the configurational parameters for the TTT and TGT segments. The band assignments and the frequency fit of the phase III chain will be discussed for the case where the phase I and II chain parameters used in the force field refinement[11] are applied to the TTT and TGT, $TG'T$ segments, respectively. A second normal coordinate calculation was done for a phase III chain which has the average of the bond angle parameters for the TTT and TGT segments found in the crystal structure work of Weinhold *et al.*[10] The *trans* internal rotation angle was taken to be 180° rather than 170.4° or 171.5° so that the calculation could be compared to the phase I results. The *gauche* angle was taken to be 51.5°. This calculation was done in conjunction with a study of the geometric dependence of the calculated frequencies and potential energy distribution (PED) for the phase I and II conformations discussed below.

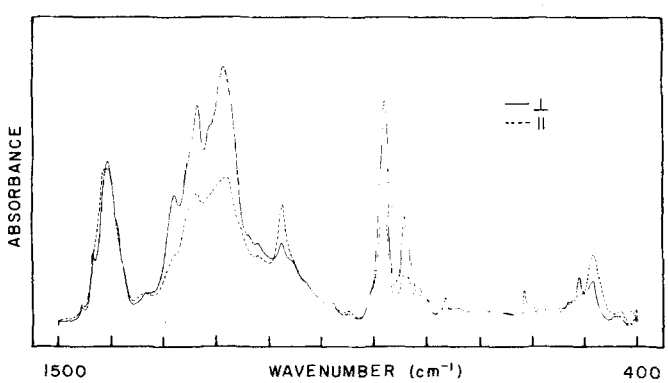

FIG. 4. Polarized infrared absorbance spectrum of phase III of poly(vinylidene fluoride): (—) electric vector perpendicular to the drawing direction; (- - -) electric vector parallel to the drawing direction.

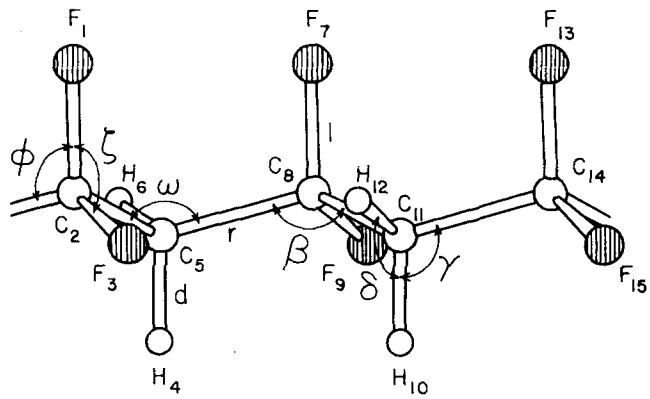

FIG. 5. Internal coordinate definitions for poly(vinylidene fluoride). Shaded atoms are fluorine.

RESULTS AND DISCUSSION

Phase I

The factor group of the line group for an isolated chain of phase I is isomorphous to the point group C_{2v}. The secular equation is of order 18. The normal mode are distributed among the symmetry species as $\Gamma = 6A1 + 2A2 + 4B1 + 6B2$. These include the zero frequency modes from pure translation and rotation: $\Gamma_{trans} = A1 + B1 + B2$ and $\Gamma_{rot} = B2$. Therefore, the nonzero modes are distributed as follows (with activity and polarization): $\Gamma_n = 5A1$ (IR, Raman; ⊥) + $2A2$ (Raman) + $3B1$ (IR, Raman; ∥) + $4B2$ (IR, Raman; ⊥).

The normal coordinate calculation was performed on a phase I chain, which had the configurational parameters used by Boerio and Koenig[11] for their force field refinement. The observed and calculated frequencies $(PED)_{ii}$ (diagonal force constants) and approximate normal mode assignments are given in Table II. For a discussion of the band assignments see Boerio and Koenig[11] and Kobayashi *et al.*[12]

Phase II

The factor group of the line group for an isolated chain of phase II is isomorphous to the point group C_s. The secular equation is of order 36. The normal modes are distributed among the symmetry species as $\Gamma = 18A' + 18A''$. These include the zero frequency modes from pure translation and rotation: $\Gamma_{trans} = 2A' + A''$ and $\Gamma_{rot} = A''$. Therefore, the nonzero modes are distributed as follows: $\Gamma_n = 16A'$ (IR, Raman; ∥, ⊥) + $16A''$ (IR, Raman; ⊥).

The observed and calculated frequencies $(PED)_{ii}$ and approximate normal mode assignments are given in Table III. As was the case for phase I, the configurational parameters were those used by Boerio and Koenig.[11] For a discussion of the band assignments see Boerio and Koenig[11] and Kobayashi *et al.*[12]

Phase III

The factor group of the line group for an isolated chain of phase III is isomorphous to the point group C_s. The

TABLE I. Valence force constants: definitions and values.

Diagonal[a]	Value[b]	Atoms involved	Common atoms	Example of diagonal force constant[c]
K_d	4.902	CH		C5–H4
K_r	4.413	CC		C2–C5
K_l	5.960	CF		C2–F1
H_γ	0.615	CCH		C2–C5–H4
H_δ	0.481	CH_2		H4–C5–H6
$H_\omega = H_\beta$	1.248	CCC		C2–C5–C8
H_ϕ	1.262	CCF		C5–C2–F1
H_ζ	1.280	CF_2		F1–C2–F3
H_τ	0.050	CCCC, FCCH (*trans*)	CC	C5–C8–C11–C14, F7–C8–C11–H10, F9–C8–C11–H12

Interaction[a]	Value[b]	Atoms involved	Common atoms	Example of interaction force constant[c]	
F_{rl}	0.740	CC, CF	C	C5–C2	C2–F1
F_r	0.148	CC, CC	C	C2–C5	C5–C8
F_l	0.621	CF, CF	C	C2–F1	C2–F3
F_d	0.058	CH, CH	C	C5–H4	C5–H6
$F_{r\gamma}$	0.206	CC, CCH	CC	C2–C5	C2–C5–H4
$F_{r\omega} = F_{r\beta}$	0.273	CC, CCC	CC	C2–C5	C2–C5–C8
$F_{r\phi}$	0.567	CC, CCF	CC	C5–C8	C5–C8–F7
$F_{l\zeta}$	0.674	CF, CF_2	CF	C8–F7	F7–C8–F9
$F_{l\phi}$	0.500	CF, CCF	CF	C8–F7	C5–C8–F7
F_ϕ	0.178	CCF, CCF	CC	C5–C8–F7	C5–C8–F9
F'_ϕ	0.143	CCF, CCF	CF	C5–C8–F7	C11–C8–F7
F_γ	0.105	CCH, CCH	CC	C8–C5–H4	C8–C5–H6
F'_γ	0.074	CCH, CCH	CH	C8–C5–H4	C2–C5–H4
$f^t_{\omega\beta}$	−0.036	CCC, CCC	CC	C5–C8–C11	C8–C11–C14
$f^g_{\beta\gamma}$	0.106	CCC, CCH	CC	C11–C8–C5	C8–C5–H4
$f^g_{\omega\phi}$	−0.085	CCC, CCF	CC	C2–C5–C8	C5–C8–H7
$f^t_{\phi\gamma}$	0.063	CCF, CCH	CC	C5–C8–F7	C8–C5–H4
$f^g_{\phi\gamma}$	0.055	CCF, CCH	CC	C5–C8–F9	C8–C5–H4
$f^g_{\omega\beta}$	−0.064	CCC, CCC	CC	C2–C5–C8	C5–C8–C11
$f^t_{\beta\gamma}$	0.207	CCC, CCH	CC	C11–C8–C5	C8–C5–H6
$f^t_{\omega\phi}$	0.239	CCC, CCF	CC	C2–C5–C8	C5–C8–F9

[a]Force constants transferred from Ref. 11.
[b]Stretch constants have units of mdyn/Å; stretch–bend interactions have units of mdyn/rad; bending constants have units of mdyn Å/rad^2.
[c]For the labeling of the atoms see Fig. 5.

secular equation is of order 72. The normal modes are distributed among the symmetry species as $\Gamma = 36A' + 36A''$. These include the zero frequency modes from pure translation and rotation; $\Gamma_{trans} = 2A' + A''$ and $\Gamma_{rot} = A''$. Therefore, the nonzero normal modes are distributed as follows: $\Gamma_n = 34A'$ (IR, Raman; ∥, ⊥) + $34A''$ (IR, Raman; ⊥).

The normal coordinate calculation was performed on a phase III chain which has the configurational parameters used by Boerio and Koenig[11] for phase I and phase II, for the *TTT* segments and *TGT*, *TG'T* segments, respectively. The observed and calculated frequencies $(PED)_{ii}$ and the approximate normal mode assignments are given in Table IV. A discussion of the band assign-

TABLE II. Observed and calculated frequencies, potential energy distribution $(PED)_{ii}$ and the approximate normal mode assignments of phase I of poly(vinylidene fluoride). CCC bond angles were 113.1° and the CH_2 and CH_2 bond angles were 109.5°.

Species	Number	Observed frequency (cm^{-1})	Calculated frequency (cm^{-1})	$(PED)_{ii}$ (%)[a]	Approximate normal mode assignment[b]
$A1$	ν_1	511	516	$H_\xi(77)+H_\phi(16)$	$\delta(CF_2)$
	ν_2	882	886	$K_l(59)$	$\nu_s(CF_2)$
	ν_3	1185	1185	$H_\omega(47)+K_l(45)+K_r(43)+H_\xi(13)$	$\delta(CCC)+\nu_s(CF_2)+\nu_s(CC)$
	ν_4	1432	1434	$H_\delta(72)+H_\gamma(17)$	$\delta(CH_2)$[c]
	ν_5	2982	2980	$K_d(98)$	$\nu_s(CH_2)$
$A2$	ν_1	Inactive	270	$H_\phi(133)$	$t(CF_2)$
	ν_2	Inactive	991	$H_\gamma(138)$	$t(CH_2)$
$B1$	ν_1	470	484	$H_\phi(78)$	$w(CH_2)$
	ν_2	1074	1063	$K_r(71)+H_\gamma(27)+H_\phi(25)$	$\nu_a(CC)+w(CH_2)+w(CF_2)$
	ν_3	1403	1398	$H_\gamma(72)+K_r(47)$	$w(CH_2)$[c]$+\nu_a(CC)$
$B2$	ν_1	448	483	$H_\phi(67)+H_\tau(18)+H_\gamma(13)$	$r(CF_2)+\tau+r(CH_2)$
	ν_2	842	843	$H_\gamma(58)+K_l(26)$	$r(CH_2)+\nu_a(CF_2)$
	ν_3	1278	1257	$K_l(93)+H_\phi(27)+H_\gamma(16)$	$\nu_a(CF_2)+r(CF_2)+r(CH_2)$
	ν_4	3019	3020	$K_d(101)$	$\nu_a(CH_2)$

[a]Only the diagonal force constants which contribute to the $(PED)_{ii}$ by 10% or greater are shown. The sum of the $(PED)_{ii}$ for the diagonal force constants may be greater than 100% because of contributions from interaction terms.
[b]Based on the $(PED)_{ii}$ and the Cartesian displacement coordinates. ν, δ, t, w, r, and τ denote stretching, bending (scissoring), twisting, wagging, rocking, and torsional modes, respectively; s and a represent symmetric, and antisymmetric, respectively.
[c]See the text on geometric sensitivity of CH_2 bending and wagging modes.

ments follows.

CF_2 stretching modes

In the frequency range 1170–1300 cm^{-1}, five bands are observed at 1176 (s, $\perp$), 1235 (s, $\perp$), 1250 (sh), 1278 (s, $\perp$), and 1297 (sh) cm^{-1}. For phase III, the CF_2 stretching modes of the A'' species are strictly of perpendicular dichroism. The out-of-phase symmetric and antisymmetric CF_2 stretches are both strictly of perpendicular dichroism and belong to the A'' species. Because of the orientation of the CF_2 groups with respect to the chain axis, the A' modes will be a mixture of perpendicular and parallel dichroism. The in-phase symmetric and antisymmetric CF_2 stretching modes will be a mixture of perpendicular and parallel dichroism and so belong to the A' species. The amount of perpendicular and parallel character will depend upon the exact geometry of the chain. For the geometry used in this study, the in-phase antisymmetric motion will exhibit predominately perpendicular dichroism, while the in-phase symmetric motion will be a combination of perpendicular and parallel dichroism.

The $\nu_{25}(A')$ mode calculated at 1251 cm^{-1} is predominately an in-phase antisymmetric CF_2 stretching mode. This band is assigned to the observed band 1250 (sh) cm^{-1}. This band could be associated with the $\nu_3(B2)$ [1278 (s, $\perp$) cm^{-1}] phase I band.

The $\nu_{24}(A'')$ mode calculated at 1182 cm^{-1} is predominately an out-of-phase symmetric CF_2 stretching mode. This mode is assigned to the observed band at 1176 (s, $\perp$) cm^{-1}. It is associated with the $\nu_{11}(A'')$ [1185 (s, $\perp$) cm^{-1}] phase II band and also with the $\nu_3(A1)$ [1185 (s, $\perp$) cm^{-1}] phase I band.

The $\nu_{25}(A'')$ mode calculated at 1251 cm^{-1} is predominately an out-of-phase antisymmetric CF_2 stretching mode which is localized in the TTT segments. This mode is assigned to the observed band 1235 (s, $\perp$) cm^{-1}. This band could be associated with the $\nu_3(B2)$ [1278 (s, $\perp$) cm^{-1}] phase I band, or the $\nu_{12}(A'')$ [1218 (s, $\perp$) cm^{-1}] phase II band.

The two remaining observed bands associated with CF_2 stretching modes [1278 (s, $\perp$) and 1297 (sh) cm^{-1}] are assigned to the two modes $\nu_{26}(A')$ and $\nu_{26}(A'')$ calculated at 1277 and 1282 cm^{-1}, respectively. The $\nu_{26}(A')$ mode is a mixture of in-phase antisymmetric CF_2 stretching modes localized in the TGT segments and in-phase symmetric CF_2 stretching mode localized in the TTT segments. The $\nu_{26}(A'')$ mode is a mixture of out-of-phase antisymmetric CF_2 stretching mode localized in the TGT segments and the out-of-phase symmetric CF_2 stretching mode localized in the TTT segments.

TABLE III. Observed and calculated frequencies, potential energy distribution $(PED)_{ii}$, and the approximate normal mode assignments of phase II of poly(vinylidene fluoride). The CCC bond angles were 115.6° and the CH_2 and CF_2 bond angles were 109.5°, with $G = 60°$.

Species	Number	Observed frequency (cm^{-1})	Calculated frequency (cm^{-1})	$(PED)_{ii}$ (%)[a]	Approximate normal mode assignment[b]
A'	ν_1		94	$H_\tau(65)+H_\omega(18)+H_\phi(16)$	$\tau+\delta(CCC)$
	ν_2		230	$H_\phi(78)+H_\omega(29)$	$t(CF_2)_i+\delta(CCC)$
	ν_3		303	$H_\phi(83)+H_\omega(14)$	$t(CF_2)_i+\delta(CCC)$
	ν_4		432	$H_\phi(51)+H_\xi(18)+H_\tau(10)+K_\tau(10)$	$r(CF_2)_o+\delta(CF_2)_1$
	ν_5	490	513	$H_\phi(44)+H_\xi(31)$	$w(CF_2)_i+\delta(CF_2)_i$
	ν_6	615	617	$H_\phi(24)+H_\xi(21)+H_\omega(14)+K_\tau(14)+H_\gamma(10)$	$w(CF_2)_i+\delta(CF_2)_i+\delta(CCC)$
	ν_7	856	836	$H_\gamma(54)+K_I(15)+H_\phi(13)$	$r(CH_2)_o+\nu_a(CF_2)_i+w(CF_2)_i$
	ν_8	875	870	$K_\tau(29)+K_I(24)+H_\omega(13)+H_\phi(10)$	$\nu_s(CC)_i+\nu_s(CF_2)_i+\delta(CCC)$
	ν_9	977	967	$H_\gamma(94)+K_I(34)$	$t(CH_2)_i+\nu_s(CF_2)_i$
	ν_{10}	1073	1070	$H_\tau(47)+K_I(41)+K_\tau(26)+H_\omega(10)$	$w(CH_2)_i+\nu_s(CF_2)_i+\nu(CC)$
	ν_{11}	1152	1156	$K_\tau(57)+H_\gamma(27)+K_I(21)+H_\phi(20)$	$\nu_a(CC)_i+w(CH_2)_i+\nu_s(CF_2)_i$
	ν_{12}	1294	1288	$K_I(79)+H_\phi(24)+H_\gamma(10)$	$\nu_a(CF_2)_i+r(CH_2)_o$
	ν_{13}	1407	1403	$H_\delta(54)+H_\gamma(34)+K_\tau(12)$	$\}$[c] $\delta(CH_2)$, $w(CH_2)$
	ν_{14}	1426	1429	$H_\gamma(54)+K_\tau(30)+H_\delta(21)$	
	ν_{15}	2989	2978	$K_d(98)$	$\nu_s(CH_2)_i$
	ν_{16}	3029	3020	$K_d(101)$	$\nu_a(CH_2)_i$
A''	ν_1		140	$H_\omega(41)+H_\tau(38)+H_\phi(35)$	$\delta(CCC)+\tau$
	ν_2		275	$H_\phi(70)+K_\tau(12)$	$t(CH_2)_o+\nu(CC)$
	ν_3		367	$H_\phi(71)+H_\omega(14)$	$t(CF_2)_o+\delta(CCC)$
	ν_4		435	$H_\phi(77)+H_\tau(15)$	$r(CF_2)_1$
	ν_5	533	522	$H_\xi(67)+H_\phi(16)$	$\delta(CF_2)_o$
	ν_6	765	776	$K_I(33)+H_\phi(31)+H_\omega(19)+K_\tau(11)$	$\nu_s(CF_2)_o+w(CF_2)_o$
	ν_7	797	818	$H_\gamma(71)+H_\phi(15)$	$r(CH_2)_i$
	ν_8		908	$K_\tau(48)+K_I(17)$	$\nu_a(CC)_o+\nu_s(CF_2)_o$
	ν_9		956	$H_\gamma(100)+K_I(26)$	$t(CH_2)_o+\nu_a(CF_2)_o$
	ν_{10}		1059	$K_\tau(93)+H_\phi(30)+K_I(14)$	$\nu_s(CC)_o$
	ν_{11}	1185	1176	$K_I(44)+H_\gamma(39)+H_\omega(22)+K_\tau(20)+H_\xi(10)$	$\nu_s(CF_2)_o+t(CH_2)_o$
	ν_{12}	1218	1257	$K_I(71)+H_\gamma(32)+H_\phi(15)$	$\nu_a(CF_2)_o+w(CH_2)_o$
	ν_{13}	1385	1388	$H_\gamma(51)+H_\delta(26)+K_\tau(15)+K_I(11)$	$\}$[c] $\delta(CH_2)$, $w(CH_2)$
	ν_{14}		1418	$H_\delta(49)+H_\gamma(32)+K_\tau(13)$	
	ν_{15}		2980	$K_d(98)$	$\nu_s(CH_2)_o$
	ν_{16}		3020	$K_d(101)$	$\nu_a(CH_2)_o$

[a] See footnote a, Table II.

[b] Based on the $(PED)_{ii}$ and the Cartesian displacement coordinates. ν, δ, t, w, r, and τ denote stretching, bending (scissoring), twisting, wagging, rocking, and torsional modes, respectively; s and a represent symmetric and antisymmetric, respectively; i and o represent in phase and out of phase, respectively.

[c] See the text on geometric sensitivity of CH_2 bending and wagging modes.

Skeletal stretching modes

In the frequency range 1000–1170 cm^{-1} four bands are observed at 1054 (w, ?), 1072 (s, ∥), 1118 (w, ?), and 1133 (w, ⊥) cm^{-1}. From the geometry of the phase III chain it can be seen that the in-phase symmetric and antisymmetric CC stretching modes are a mixture of perpendicular and parallel dichroism and belong to the A' species. The out-of-phase symmetric and antisymmetric CC stretching modes have only perpendicular dichroism and belong to the A'' species.

Two modes $\nu_{21}(A')$ and $\nu_{23}(A')$ calculated at 1057 and 1148 cm^{-1}, respectively, are predominately in-phase symmetric CC stretching modes. The $\nu_{23}(A')$ CC stretching mode is also coupled with an in-phase antisymmetric CF_2 stretching mode localized in the TGT segments. The $\nu_{21}(A')$ mode is assigned to the observed band 1054 (w, ?) cm^{-1} and the $\nu_{23}(A')$ mode is assigned to the observed band 1133 (w, ⊥) cm^{-1}.

The $\nu_{22}(A')$ mode calculated at 1070 cm^{-1} is predominately an in-phase antisymmetric CC stretching mode localized in the TGT segments. This mode is assigned to the observed band 1073(s, ∥) cm^{-1} and is associated with the $\nu_{10}(A')$[1073(s, ∥) cm^{-1}] phase II band.

The $\nu_{23}(A'')$ mode calculated at 1146 cm^{-1} is a mixture of out-of-phase symmetric CC stretching mode localized in TTT segments and out-of-phase antisymmetric CC stretching modes localized in TGT segments. This mode is assigned to the observed band at 1118(w, ?) cm^{-1}.

CH_2 twisting mode

In the frequency range 925–1000 cm^{-1} two bands are observed at 949(w, ?) and 976(w, ⊥) cm^{-1}. Two modes in this frequency range [$\nu_{19}(A')$ and $\nu_{20}(A')$ calculated at 954 and 985 cm^{-1}, respectively] are predominately in-phase CH_2 twisting modes, while the two modes $\nu_{19}(A'')$

TABLE IV. Observed and calculated frequencies, potential energy distribution $(PED)_{ii}$, and the approximate normal mode assignment of phase III of poly(vinylidene fluoride). *TTT* segments with CCC bond angles of 113.1°; *TGT* segments with CCC bond angles of 115.6°, $G = 60°$. All CH_2 and CF_2 bond angles were 109.5°.

Species	Number	Observed frequency (cm^{-1})	Calculated frequency (cm^{-1})	$(PED)_{ii}$ (%)[a]	Approximate normal mode assignment[b]
A'	ν_1		50	$H_\tau(93)$	τ
	ν_2		65	$H_\tau(75)+H_\omega(12)$	τ
	ν_3		98	$H_\omega(50)+H_\tau(29)+H_\phi(14)$	$\delta(CCC)+\tau$
	ν_4		141	$H_\tau(36)+H_\omega(31)+H_\phi(20)+K_\tau(11)$	$\tau+\delta(CCC)$
	ν_5		165	$H_\omega(51)+H_\phi(38)+K_\tau(20)$	$\delta(CCC)+t(CF_2)_1$
	ν_6		276	$H_\phi(125)$	$t(CF_2)_1$
	ν_7		305	$H_\phi(55)+H_\omega(18)+H_\zeta(10)$	$t(CF_2)_1+\delta(CCC)$
	ν_8		373	$H_\phi(78)$	$t(CF_2)_i$
	ν_9		418	$H_\phi(87)+H_\tau(12)$	$r(CH_2)_o+\tau$
	ν_{10}	440	466	$H_\phi(65)+H_\tau(15)$	$r(CF_2)_o+\tau$
	ν_{11}	483	501	$H_\phi(44)+H_\zeta(30)$	$w(CF_2)_1$ (II) $+\delta(CF_2)_i$ (I)
	ν_{12}		543	$H_\zeta(53)+H_\phi(19)$	$\delta(CH_2)_i+w(CF_2)_i$ (II)
	ν_{13}	550	545	$H_\zeta(43)+H_\phi(34)$	$\delta'(CH_2)_i+w(CF_2)_i$
	ν_{14}	775	812	$H_\gamma(41)+K_l(21)+H_\phi(15)+K_\tau(14)$	$r(CH_2)_o+\nu_s'(CF_2)_i+w(CF_2)_i$ (I)
	ν_{15}	813	820	$H_\gamma(35)+H_\phi(24)+H_\omega(15)+K_\tau(10)$	$r(CH_2)_o+w'(CF_2)_i+\delta(CCC)$ $+\nu(CC)$
	ν_{16}	835	834	$H_\gamma(60)+K_l(21)$	$r(CH_2)_o+\nu_a(CF_2)_i$
	ν_{17}	883	876	$K_l(48)+K_\tau(13)$	$\nu_s(CF_2)_i+\nu(CC)$
	ν_{18}		915	$K_\tau(46)+K_l(17)$	$\nu_s(CC)_i+\nu_s'(CF_2)_i$
	ν_{19}		954	$H_\gamma(99)+K_l(26)$	$t'(CH_2)_i+\nu_a'(CF_2)_i$
	ν_{20}		985	$H_\gamma(124)$	$t(CH_2)_i$
	ν_{21}	1054	1057	$K_\tau(75)+H_\phi(24)+H_\gamma(17)+K_l(15)$	$\nu_s(CC)_i+w'(CF_2)_i+w(CH_2)_i$ $+\nu_a(CF_2)_i$ (II) $+\nu_s(CF_2)_i$ (I)
	ν_{22}	1073	1070	$K_\tau(64)+K_l(28)+H_\gamma(19)+H_\phi(12)$	$\nu_a(CC)_i$ (II) $+\nu_s'(CF_2)_i$ $+w(CH_2)_i$
	ν_{23}	1133	1148	$K_\tau(48)+K_l(42)+H_\omega(25)+H_\phi(15)$	$\nu_s(CC)_i+\nu_a(CF_2)_i$ (II) $+\nu_s(CF_2)_i$ (I) $+\delta(CCC)_i$ (I) $+w(CF_2)_i$ (II)
	ν_{24}		1167	$K_l(38)+K_\tau(35)+H_\gamma(28)+H_\omega(16)+H_\phi(10)$	$\nu_s(CH_2)_i$ (II) $+\nu(CC)$ $+t(CH_2)_i$ (II)
	ν_{25}	1250	1251	$K_l(90)+H_\gamma(26)+H_\phi(22)$	$\nu_a'(CF_2)_i$ (I) $+r(CH_2)_o+t'(CH_2)_i$
	ν_{26}	1278	1277	$K_l(70)+H_\gamma(23)+H_\phi(18)+H_\omega(11)$	$\nu_a(CF_2)_i$ (II) $+\nu_s(CF_2)_i$ (I) $+w'(CH_2)_i$
	ν_{27}		1356	$H_\gamma(77)+K_\tau(22)$	c
	ν_{28}		1405	$H_\delta(74)+H_\gamma(18)$	$\delta(CH_2)$, $w(CH_2)$
	ν_{29}		1411	$H_\gamma(57)+K_\tau(38)+H_\delta(22)$	
	ν_{30}		1430	$H_\delta(52)+H_\gamma(32)+K_\tau(14)$	
	ν_{31}		2979	$K_d(98)$	$\nu_s'(CH_2)_i$
	ν_{32}		2979	$K_d(98)$	$\nu_s(CH_2)_i$
	ν_{33}		3019	$K_d(101)$	$\nu_a'(CH_2)_i$
	ν_{34}		3020	$K_d(101)$	$\nu_a(CH_2)_i$
A''	ν_1		50	$H_\tau(89)$	τ
	ν_2		79	$H_\tau(47)+H_\omega(36)+H_\phi(10)+H_\gamma(10)$	$\tau+\delta(CCC)$
	ν_3		106	$H_\tau(66)+H_\phi(15)+H_\omega(12)+H_\gamma(11)$	τ
	ν_4		169	$H_\omega(62)+H_\phi(50)$	$\delta(CCC)+t(CH_2)_o$
	ν_5		233	$H_\phi(38)+H_\omega(26)+K_\tau(22)$	$t(CH_2)_o+\delta(CCC)$
	ν_6		275	$H_\phi(68)+H_\omega(26)$	$t(CH_2)_o+\delta(CCC)$
	ν_7		303	$H_\phi(114)$	$t(CF_2)_o$ (II)
	ν_8		347	$H_\phi(75)$	$t(CF_2)_o$
	ν_9	430	439	$H_\phi(71)+H_\tau(16)$	$r'(CF_2)_i+\tau$
	ν_{10}		467	$H_\phi(71)+H_\tau(17)+H_\gamma(10)$	$r(CF_2)_i+\tau$
	ν_{11}	512	508	$H_\zeta(70)+H_\phi(13)$	$\delta(CH_2)_o$
	ν_{12}	534	530	$H_\zeta(59)+H_\omega(16)+H_\phi(10)$	$\delta(CF_2)_o+\delta(CCC)$
	ν_{13}	613	625	$H_\phi(49)+K_\tau(22)+H_\omega(11)$	$w(CH_2)_o+\nu(CC)+\delta(CCC)$
	ν_{14}	764	733	$K_\tau(41)+H_\phi(29)$	$\nu_s(CC)_o$ (II) $+w(CF_2)_o$
	ν_{15}	797	824	$H_\gamma(62)+H_\phi(14)+K_l(12)$	$r'(CH_2)_i+w(CF_2)_o$ (II) $+\nu_a(CF_2)_o$
	ν_{16}	840	835	$H_\gamma(62)+K_l(18)+H_\phi(11)$	$r(CH_2)_i+\nu_a(CF_2)_o$ (I)
	ν_{17}	857	858	$K_\tau(33)+K_l(21)+H_\omega(15)$	$\nu_a(CC)_o+\nu_s(CF_2)_o$ (II) $+\delta(CCC)$
	ν_{18}	895	889	$K_l(46)+K_\tau(17)$	$\nu_s(CF_2)_o$ (I) $+\nu(CC)$
	ν_{19}		963	$K_\gamma(101)+K_l(27)$	$t(CH_2)_o+\nu_s(CF_2)_o$ (II) $+\nu_a(CF_2)_o$ (I)

TABLE IV (*Continued*)

Species	Number	Observed frequency (cm^{-1})	Calculated frequency (cm^{-1})	$(PED)_{ii}$ (%)[a]	Approximate normal mode assignment[b]
A''	ν_{20}	976	977	$H_\gamma(122)+K_t(10)$	$t(CH_2)_o+\nu_a(CF_2)_o$
	ν_{21}		1053	$K_r(48)+K_t(41)+H_\gamma(19)+H_\phi(12)$	$\nu_s(CC)_o$ (II) $+\nu_s(CF_2)_o$ $+w(CH_2)_o$ (I) $+t(CH_2)_o$ (II)
	ν_{22}		1076	$K_r(61)+K_t(26)+H_\gamma(21)+H_\phi(18)$	$\nu_a(CC)_o+\nu_s(CH_2)_o+w(CH_2)_o$
	ν_{23}	1118	1146	$K_r(66)+H_\phi(22)+H_\gamma(17)+K_t(16)$	$\nu_s(CC)_o$ (I) $+\nu_a(CC)_o$ (II) $+w(CF_2)_o+w(CH_2)_o$ $+\nu_s(CF_2)_o$
	ν_{24}	1176	1182	$K_t(47)+K_r(31)+H_w(30)+H_\gamma(22)+H_\zeta(10)$	$\nu_s(CF_2)_o+\nu(CC)+\delta(CCC)$ $+t(CH_2)_o$
	ν_{25}	1235	1251	$K_t(91)+H_\gamma(25)+H_\phi(22)$	$\nu_a(CF_2)_o$ (I) $+t(CH_2)_o$ $+r(CH_2)_i$ (II)
	ν_{26}	1297	1282	$K_t(72)+H_\phi(21)+H_\gamma(14)+K_r(12)+H_\omega(10)$	$\nu_a(CF_2)_o$ (II) $+\nu_s(CF_2)_o$ (I) $+t(CH_2)_o$ (I) $+w(CH_2)_o$ (II)
	ν_{27}		1368	$H_\gamma(76)+K_r(29)$	
	ν_{28}		1405	$H_\gamma(48)+H_\delta(23)+K_r(22)$	[c]
	ν_{29}		1407	$H_\delta(47)+H_\gamma(38)+K_r(14)$	$\delta(CH_2)$, $w(CH_2)$
	ν_{30}		1428	$H_\delta(65)+H_\gamma(22)$	
	ν_{31}		2978	$K_d(98)$	$\nu_s(CH_2)_o$
	ν_{32}		2980	$K_d(98)$	$\nu_s(CH_2)_o$
	ν_{33}		3020	$K_d(101)$	$\nu_a(CH_2)_o$
	ν_{34}		3020	$K_d(101)$	$\nu_a(CH_2)_o$

[a]See footnote a Table II.

[b]Based on the $(PED)_{ii}$ and Cartesian displacement coordinates, ν, δ, t, w, r, and τ denote stretching, bending (scissoring); twisting, wagging, rocking, and torsional modes, respectively; s and a represent symmetric and antisymmetric, respectively; i and o represent in phase and out of phase, respectively; primes indicate that the TTT and TGT segments vibrate out of phase; (I) and (II) indicate that the motion is localized in the TTT or TGT segments, respectively.

[c]See the text on geometric sensitivity of CH_2 bending and wagging modes.

and $\nu_{20}(A'')$ calculated at 963 and 977 cm^{-1}, respectively, are predominately out-of-phase CH_2 twisting modes. The $\nu_{20}(A'')$ mode is assigned to the observed band 976(w, $\perp$) cm^{-1}.

The band observed at 949(w, ?) cm^{-1} could be assigned to $\nu_{19}(A')$; however, this weak band is thought to be due to head-to-head followed by tail-to-tail (HHTT) defects based on the IR and Raman spectra of the alternating copolymer of ethylene and tetrafluoroethylene of Kobayashi *et al.*[12]

CF_2 stretching modes coupled with skeletal stretching modes

In the frequency range 850–925 cm^{-1} three bands are observed at 857(w, $\perp$), 883(s, $\perp$), and 895(sh) cm^{-1}. Two modes [$\nu_{17}(A'')$ and $\nu_{18}(A'')$ calculated at 858 and 889 cm^{-1}, respectively] are out-of-phase symmetric CF_2 stretching modes coupled with skeletal stretching modes. These two bands are assigned to the observed bands 857(w, $\perp$) and 895(sh) cm^{-1}, respectively. The CF_2 stretching mode component of $\nu_{17}(A'')$ is localized in the phase II regions, while the CF_2 stretching component of $\nu_{18}(A'')$ is localized in the phase I regions. The $\nu_{18}(A'')$ mode is associated with the $\nu_2(A1)$[882(s, $\perp$) cm^{-1}] phase I band.

Two modes [$\nu_{17}(A')$ and $\nu_{18}(A')$ calculated at 876 and 915 cm^{-1}, respectively] are in-phase symmetric CF_2 stretching modes coupled with skeletal stretching modes. The $\nu_{17}(A')$ mode is assigned to the observed band 883(s, $\perp$) cm^{-1}, which is associated with the $\nu_8(A')$[875(s, $\perp$) cm^{-1}] phase II band.

CH_2 rocking mode

In the frequency range 770–850 cm^{-1} five bands are observed at 775(w, $\parallel$), 797(w, ?), 813(m, $\perp$), 835(m, $\perp$), and 840(m, $\perp$) cm^{-1}. From the geometry of the phase III chain it can be seen that the out-of-phase rocking mode is a mixture of perpendicular and parallel dichroism and belongs to the A' species. The in-phase rocking mode has only perpendicular dichroism and belongs to the A'' species.

Three of the modes [$\nu_{14}(A')$, $\nu_{15}(A')$, and $\nu_{16}(A')$ calculated at 812, 820, and 834 cm^{-1}, respectively] are predominately out-of-phase CH_2 rocking modes. The three modes are assigned to the observed bands 775(w, $\parallel$), 813(m, $\perp$), and 835(m, $\perp$) cm^{-1}, respectively. The $\nu_{16}(A')$ mode is associated with the $\nu_7(A')$[856(m, $\perp$) cm^{-1}] phase II band.

The two remaining modes $\nu_{15}(A'')$ and $\nu_{16}(A'')$ calculated at 824 and 835 cm^{-1}, respectively, are predominately in-phase CH_2 rocking modes. These two bands are assigned to the bands observed at 797(w, ?) and 840(m, $\perp$) cm^{-1}, respectively. The $\nu_{15}(A'')$ mode is associated with the $\nu_7(A'')$[797(s, $\perp$) cm^{-1}] phase II band. The $\nu_{16}(A'')$ mode is associated with the $\nu_2(B2)$[842(s, $\perp$) cm^{-1}] phase I band.

CH_2 bending and CF_2 wagging modes

In the frequency range 475–770 cm^{-1} six bands are observed at 483(s, ∥), 512(s, ⊥), 534(w, ⊥), 550(sh), 613(m, ∥), and 764(m, ⊥) cm^{-1}. From the geometry of the phase III chain it can be seen that the in-phase wagging mode has only parallel dichroism and belongs to the A' species. The out-of-phase wagging mode has only perpendicular dichroism and belongs to the A'' species. The in-phase bending mode has both perpendicular and parallel dichroism and belongs to the A' species. The out-of-phase bending mode has only perpendicular dichroism and belongs to the A'' species.

Two modes [$\nu_{11}(A'')$ and $\nu_{12}(A'')$ calculated at 508 and 530 cm^{-1}, respectively] are predominately out-of-phase CF_2 bending modes. The $\nu_{11}(A'')$ mode is assigned to the observed band at 512(s, ⊥) cm^{-1} and is associated with the $\nu_1(A1)$[511(s, ⊥) cm^{-1}] phase I band. The $\nu_{12}(A'')$ mode is assigned to the observed band at 534(w, ⊥) cm^{-1} and is associated with the $\nu_5(A'')$[533(s, ⊥) cm^{-1}] phase II band.

The $\nu_{13}(A')$ mode calculated at 545 cm^{-1} is predominately an in-phase CF_2 bending mode with the TTT and TGT segments out of phase. This mode is assigned to the observed band 550(sh) cm^{-1}.

The $\nu_{11}(A')$ mode calculated at 501 cm^{-1} is a mixture of an in-phase CF_2 wagging mode which is localized in the TGT segments and an in-phase CF_2 bending mode which is localized in the TTT segments. The $\nu_{11}(A')$ band is assigned to the observed band at 483(s, ∥) cm^{-1}, and is associated with the $\nu_5(A')$[490(s, ∥) cm^{-1}] phase II band.

The $\nu_{14}(A'')$ mode calculated at 733 cm^{-1} is a mixture of an out-of-phase CC stretching mode which is localized in the TGT segments and an out-of-phase CF_2 wagging mode. The $\nu_{14}(A'')$ mode is assigned to the observed band at 764(m, ⊥) cm^{-1}. This mode is associated with the $\nu_6(A'')$[765(s, ⊥) cm^{-1}] phase II band.

The $\nu_{13}(A'')$ mode calculated at 625 cm^{-1} is predominately an out-of-phase CF_2 wagging mode which is coupled with skeletal deformations, and is predicted to have perpendicular dichroism. This mode is isolated from neighboring calculated bands $\nu_{13}(A')$ and $\nu_{14}(A'')$ by 80 and 108 cm^{-1}, respectively. We are forced, therefore, to assign $\nu_{13}(A'')$ to the band observed at 613(m, ∥) cm^{-1} even though the observed band has parallel dichroism and so should be an A' species. This band is associated with the $\nu_6(A')$[615(s, ∥) cm^{-1}] phase II band which is an in-phase CF_2 wagging mode coupled with an in-phase CF_2 bending mode and skeletal deformations. Presumably, this band is calculated as an out-of-phase wagging mode (A'' species) rather than an in-phase wagging mode (A' species) because of the incompleteness of the valence force field. The intermolecular force constants evidently need to be taken into account, along with intramolecular valence force constants which extend further than the nearest-neighbor interaction force constants used in this study.

CF_2 rocking mode

In the frequency range 400–475 cm^{-1} two bands are observed at 430(w, ?) and 440(w, ?) cm^{-1}. The $\nu_9(A'')$ mode calculated at 439 cm^{-1} is predominately an in-phase CF_2 rocking mode with the TTT and TGT segments out of phase. The $\nu_9(A'')$ mode is assigned to the observed band at 430(w, ?) cm^{-1}.

The $\nu_{10}(A')$ mode calculated at 466 cm^{-1} is predominately an out-of-phase CF_2 rocking mode. The $\nu_{10}(A')$ mode is assigned to the observed band at 440(w, ?) cm^{-1}. This band is associated with the $\nu_1(B2)$[448(w, ⊥) cm^{-1}] phase I band.

TABLE V. Geometric dependence of the calculated frequencies and potential energy distribution $(PED)_{ii}$ of phase I of poly(vinylidene fluoride). The two extremes in CCC bond angle are presented, holding CH_2 and CF_2 bond angles at 109.5°.

Species and number		∠CCC = 110° Frequency (cm^{-1})	∠CCC = 110° $(PED)_{ii}$ (%)[a]	∠CCC = 120° Frequency (cm^{-1})	∠CCC = 120° $(PED)_{ii}$ (%)[a]
A1	ν_1	522	H_ξ(75) + H_ϕ(17)	507	H_ξ(80) + H_ϕ(14)
	ν_2	890	K_l(59)	878	K_l(57) + H_ω(10)
	ν_3	1186	K_r(47) + H_ω(46) + K_l(44) + H_ξ(13)	1185	K_r(34) + H_ω(49) + K_l(46) + H_ξ(13)
	ν_4	1451	H_δ(71) + H_γ(18)	1400	H_δ(75) + H_γ(13)
	ν_5	2981	K_d(98)	2980	K_d(98)
A2	ν_1	267	H_ϕ(132)	278	H_ϕ(133)
	ν_2	979	H_γ(137)	1015	H_γ(138)
B1	ν_1	477	H_ϕ(77)	501	H_ϕ(81)
	ν_2	1044	K_r(71) + H_γ(27) + H_ϕ(26)	1103	K_r(71) + H_γ(28) + H_ϕ(22)
	ν_3	1382	H_γ(72) + K_r(46)	1430	H_γ(71) + K_r(49)
B2	ν_1	493	H_ϕ(68) + H_γ(13) + H_τ(16)	461	H_ϕ(62) + H_γ(14) + H_τ(23)
	ν_2	860	H_γ(58) + K_l(29)	808	H_γ(56) + K_l(22) + H_ϕ(11)
	ν_3	1263	K_l(90) + H_ϕ(28) + H_γ(18)	1245	K_l(98) + H_ϕ(26) + H_γ(14)
	ν_4	3020	K_d(101)	3020	K_d(101)

[a]See footnote a, Table II.

TABLE VI. Geometric dependence of the calculated frequencies and potential energy distribution $(PED)_{ii}$ of phase I of poly(vinylidene fluoride). The two extremes in CH_2 and CF_2 bond angles are presented, holding CCC bond angles at 117.6°.

Species and number		$\angle CH_2 = \angle CF_2 = 102°$		$\angle CH_2 = \angle CF_2 = 108°$	
		Frequency (cm^{-1})	$(PED)_{ii}$ [a]	Frequency (cm^{-1})	$(PED)_{ii}$ [a]
$A1$	ν_1	492	$H_\zeta(83)+H_\phi(13)$	507	$H_\zeta(80)+H_\phi(15)$
	ν_2	896	$K_l(53)+H_\omega(11)$	884	$K_l(57)$
	ν_3	1226	$K_l(52)+H_\omega(44)+K_r(34)+H_\zeta(11)$	1192	$K_l(47)+H_\omega(48)+K_r(37)+H_\zeta(12)$
	ν_4	1389	$H_\delta(76)+H_\gamma(13)$	1407	$H_\delta(75)+H_\gamma(14)$
	ν_5	2997	$K_d(98)$	2983	$K_d(98)$
$A2$	ν_1	278	$H_\phi(133)$	276	$H_\phi(133)$
	ν_2	1015	$H_\gamma(138)$	1009	$H_\gamma(138)$
$B1$	ν_1	498	$H_\phi(78)$	496	$H_\phi(80)$
	ν_2	1090	$K_r(71)+H_\gamma(27)+H_\phi(25)$	1090	$K_r(71)+H_\gamma(27)+H_\phi(27)$
	ν_3	1439	$H_\gamma(72)+K_r(47)$	1423	$H_\gamma(71)+K_r(48)$
$B2$	ν_1	462	$H_\phi(63)+H_\tau(23)+H_\gamma(13)$	467	$H_\phi(64)+H_\tau(22)+H_\gamma(14)$
	ν_2	806	$H_\gamma(56)+K_l(23)+H_\phi(10)$	817	$H_\gamma(57)+K_l(23)+H_\phi(10)$
	ν_3	1207	$K_l(96)+H_\phi(27)+H_\gamma(15)$	1241	$K_l(96)+H_\phi(26)+H_\gamma(15)$
	ν_4	3005	$K_d(101)$	3017	$K_d(101)$

[a]See footnote a, Table II.

TABLE VII. Geometric dependence of the calculated frequencies and potential energy distribution $(PED)_{ii}$ of phase II of poly(vinylidene fluoride). The two extremes in CCC bond angle are presented, holding CH_2 and CF_2 bond angles at 109.5°, with $G = 60°$.

Species and number		$\angle CCC = 113°$		$\angle CCC = 118°$	
		Frequency (cm^{-1})	$(PED)_{ii}$ [a]	Frequency (cm^{-1})	$(PED)_{ii}$ [a]
A'	ν_1	94	$H_\tau(64)+H_\omega(19)+H_\phi(16)$	93	$H_\tau(66)+H_\omega(16)+H_\phi(16)$
	ν_2	228	$H_\phi(77)+H_\omega(30)+H_\tau(10)$	232	$H_\phi(79)+H_\omega(29)$
	ν_3	300	$H_\phi(85)+H_\omega(13)$	305	$H_\phi(81)+H_\omega(14)$
	ν_4	439	$H_\phi(51)+H_\zeta(19)$	425	$H_\phi(51)+H_\zeta(17)+K_r(10)+H_\tau(12)$
	ν_5	517	$H_\phi(45)+H_\zeta(31)$	509	$H_\phi(43)+H_\zeta(31)$
	ν_6	621	$H_\phi(26)+H_\zeta(20)+H_\omega(15)+K_r(14)$	612	$H_\phi(23)+H_\zeta(23)+H_\omega(14)+K_r(14)+H_\gamma(12)$
	ν_7	848	$H_\gamma(56)+K_l(15)+H_\phi(11)$	824	$H_\gamma(52)+K_l(15)+H_\phi(15)$
	ν_8	874	$K_r(29)+K_l(27)+H_\omega(11)$	866	$K_r(29)+K_l(22)+H_\omega(14)+H_\phi(11)$
	ν_9	962	$H_\gamma(100)+K_l(29)$	971	$H_\gamma(88)+K_l(38)$
	ν_{10}	1067	$K_l(41)+H_\gamma(41)+K_r(30)+H_\omega(10)$	1074	$K_l(40)+H_\gamma(53)+K_r(22)+H_\omega(10)$
	ν_{11}	1149	$K_r(56)+H_\gamma(27)+K_l(22)+H_\phi(19)$	1163	$K_r(58)+H_\gamma(26)+K_l(20)+H_\phi(20)$
	ν_{12}	1289	$K_l(78)+H_\phi(25)+H_\gamma(10)$	1286	$K_l(78)+H_\phi(24)+H_\gamma(10)+K_r(10)$
	ν_{13}	1403	$H_\gamma(60)+H_\delta(18)+K_r(29)$	1394	$H_\gamma(21)+H_\delta(71)+K_r(5)$
	ν_{14}	1430	$H_\delta(56)+H_\gamma(29)+K_r(12)$	1435	$H_\delta(6)+H_\gamma(65)+K_r(38)$
	ν_{15}	2979	$K_d(98)$	2978	$K_d(98)$
	ν_{16}	3021	$K_d(101)$	3020	$K_d(101)$
A''	ν_1	138	$H_\omega(42)+H_\tau(37)+H_\phi(34)$	143	$H_\omega(40)+H_\tau(38)+H_\phi(35)$
	ν_2	271	$H_\phi(69)+K_r(12)$	279	$H_\phi(70)+K_r(12)$
	ν_3	372	$H_\phi(71)+H_\omega(14)$	364	$H_\phi(71)+H_\omega(13)$
	ν_4	437	$H_\phi(78)+H_\tau(14)$	432	$H_\phi(75)+H_\tau(17)$
	ν_5	523	$H_\zeta(66)+H_\phi(16)$	521	$H_\zeta(67)+H_\phi(16)$
	ν_6	773	$H_\phi(35)+K_l(30)+H_\omega(20)+K_r(10)$	778	$K_l(36)+H_\phi(27)+H_\omega(18)+K_r(12)$
	ν_7	835	$H_\gamma(73)+H_\phi(13)$	802	$H_\gamma(67)+H_\phi(19)$
	ν_8	899	$K_r(46)+K_l(18)$	916	$K_r(50)+K_l(16)$
	ν_9	949	$H_\gamma(102)+K_l(24)$	962	$H_\gamma(99)+K_l(27)$
	ν_{10}	1057	$K_r(94)+H_\phi(29)+K_l(14)$	1061	$K_r(93)+H_\phi(32)+K_l(13)$
	ν_{11}	1172	$K_l(45)+H_\gamma(38)+H_\omega(22)+K_r(21)$	1181	$K_l(44)+H_\gamma(39)+H_\omega(22)+K_r(19)$
	ν_{12}	1254	$K_l(70)+H_\gamma(34)+H_\phi(15)$	1259	$K_l(72)+H_\gamma(31)+H_\phi(15)$
	ν_{13}	1385	$H_\gamma(58)+K_r(21)+K_l(16)$	1384	$H_\delta(52)+H_\gamma(36)$
	ν_{14}	1426	$H_\delta(65)+H_\gamma(23)$	1417	$H_\gamma(48)+H_\delta(25)+K_r(19)$
	ν_{15}	2980	$K_d(98)$	2980	$K_d(98)$
	ν_{16}	3020	$K_d(101)$	3020	$K_d(101)$

[a]See footnote a, Table II.

CH_2 bending and CH_2 wagging mode

The CH_2 bending and CH_2 wagging modes are found in the frequency range 1350–1435 cm^{-1} in all four phases of PVF_2. The assignments of individual bands could not be made because of the geometric sensitivity of both the frequency and $(PED)_{ii}$, as will be discussed below.

Geometry dependence

As has been pointed out by Zerbi,[22] the geometry of a polymer must be considered when the force constants are transferred from model compounds. The force constants are geometry dependent, and the elements of the S matrix are affected by the equilibrium bond angles and internal rotation angles. A change in the geometry of the molecule will introduce changes in the elements of the S matrix, and hence in the calculated frequencies and PED. The geometrical changes can be conformational in origin, such as the molecular geometries of phases I, II, and III of PVF_2. These conformational changes will usually be accompanied by changes in the line group symmetry of the isolated polymer chain. The geometrical changes may also be configurational changes involving bond lengths, bond angles, and internal rotation angles, retaining however the conformation and hence the symmetry of the original molecule.

Geometric sensitivity of the calculated frequencies has been observed for several polymers[23–26] for which the geometry of the polymer chain differs from the geometry of the model compound from which the force field was transferred.[27,28] In the case of polyethylene[23] and the model compound for poly(vinylidene chloride), i.e., secondary dichlorides,[28] the effect of geometry changes on selected force constants was investigated. The force constants which were determined to be sensitive to various geometry changes were allowed to vary in a force field refinement, while fixing all other force constants at the zero-order values.

In this work we chose to identify which modes are sensitive to geometry changes based only on a zero-order valence force field calculation. The equilibrium

TABLE VIII. Geometric dependence of the calculated frequencies and potential energy distribution $(PED)_{ii}$ of phase II of poly(vinylidene fluoride). The two extremes in CH_2 and CF_2 bond angles are presented, holding CCC bond angles 114.9°, with $G = 51.5°$.

Species and number		$CH_2 = CF_2 = 100°$ Frequency (cm^{-1})	$(PED)_{ii}$ [a]	$CH_2 = CF_2 = 106°$ Frequency (cm^{-1})	$(PED)_{ii}$ [a]
A'	ν_1	94	$H_\tau(68)+H_\omega(15)+H_\phi(14)$	93	$H_\tau(68)+H_\omega(15)+H_\phi(15)$
	ν_2	238	$H_\phi(79)+H_\omega(29)$	236	$H_\phi(79)+H_\omega(30)$
	ν_3	298	$H_\phi(89)+H_\omega(12)$	297	$H_\phi(87)+H_\omega(13)$
	ν_4	432	$H_\phi(45)+H_\zeta(27)+H_\tau(10)$	436	$H_\phi(48)+H_\zeta(22)+H_\tau(10)$
	ν_5	499	$H_\phi(40)+H_\zeta(36)$	507	$H_\phi(43)+H_\zeta(32)$
	ν_6	614	$H_\phi(24)+K_r(20)+H_\omega(15)+H_\zeta(14)+H_\gamma(13)$	622	$H_\phi(23)+K_r(17)+H_\omega(15)+H_\zeta(18)+H_\gamma(10)$
	ν_7	830	$H_\gamma(51)+K_l(22)+H_\phi(11)$	836	$H_\gamma(55)+K_l(20)+H_\phi(11)$
	ν_8	876	$K_r(39)+H_\omega(13)+K_l(13)+H_\phi(12)$	872	$K_r(36)+H_\omega(13)+K_l(17)+H_\phi(11)$
	ν_9	989	$H_\gamma(108)+K_l(24)$	976	$H_\gamma(101)+K_l(29)$
	ν_{10}	1082	$K_l(50)+H_\gamma(37)+K_r(26)+H_\phi(11)$	1071	$K_l(48)+H_\gamma(42)+K_r(25)$
	ν_{11}	1170	$K_r(51)+K_l(39)+H_\gamma(19)+H_\phi(19)$	1161	$K_r(57)+K_l(25)+H_\gamma(19)+H_\phi(21)$
	ν_{12}	1249	$K_l(66)+H_\phi(27)+K_r(15)+H_\gamma(12)$	1272	$K_l(76)+H_\phi(26)+K_r(10)+H_\gamma(11)$
	ν_{13}	1381	$H_\delta(76)+H_\gamma(18)$	1397	$H_\delta(68)+H_\gamma(24)$
	ν_{14}	1448	$H_\gamma(70)+K_r(36)$	1432	$H_\gamma(64)+K_r(35)$
	ν_{15}	2999	$K_d(98)$	2986	$K_d(98)$
	ν_{16}	3001	$K_d(100)$	3013	$K_d(101)$
A''	ν_1	136	$H_\tau(43)+H_\omega(35)+H_\phi(30)$	135	$H_\tau(44)+H_\omega(36)+H_\phi(30)$
	ν_2	274	$H_\phi(66)+K_r(16)$	274	$H_\phi(64)+K_r(15)+H_\omega(10)$
	ν_3	379	$H_\phi(74)+H_\omega(11)$	376	$H_\phi(75)+H_\omega(11)$
	ν_4	428	$H_\phi(79)+H_\tau(15)$	430	$H_\phi(81)+H_\tau(15)$
	ν_5	494	$H_\zeta(73)+H_\phi(15)$	510	$H_\zeta(70)+H_\phi(16)$
	ν_6	785	$K_l(29)+H_\phi(28)+H_\omega(16)+H_\gamma(15)+K_r(11)$	776	$H_\phi(33)+K_l(32)+H_\omega(19)+K_r(11)$
	ν_7	807	$H_\gamma(61)+H_\phi(21)$	816	$H_\gamma(73)+H_\phi(16)$
	ν_8	901	$K_r(54)+K_l(13)$	904	$K_r(50)+K_l(15)$
	ν_9	961	$H_\gamma(97)+K_l(31)$	956	$H_\gamma(100)+K_l(28)$
	ν_{10}	1067	$K_r(92)+H_\phi(32)+K_l(12)$	1061	$K_r(94)+H_\phi(31)+K_l(12)$
	ν_{11}	1199	$K_l(69)+H_\gamma(41)+K_r(12)+H_\phi(10)$	1191	$K_l(51)+H_\gamma(36)+K_r(18)+H_\omega(21)$
	ν_{12}	1243	$K_l(56)+H_\gamma(25)+H_\omega(25)$	1246	$K_l(71)+H_\gamma(30)+H_\omega(15)+H_\phi(15)$
	ν_{13}	1379	$H_\delta(68)+H_\gamma(23)$	1388	$H_\delta(43)+H_\gamma(41)+K_r(11)$
	ν_{14}	1420	$H_\gamma(63)+K_r(25)$	1417	$H_\gamma(43)+H_\delta(32)+K_r(19)$
	ν_{15}	3000	$K_d(100)$	2988	$K_d(98)$
	ν_{16}	3002	$K_d(100)$	3013	$K_d(101)$

[a]See footnote a, Table II.

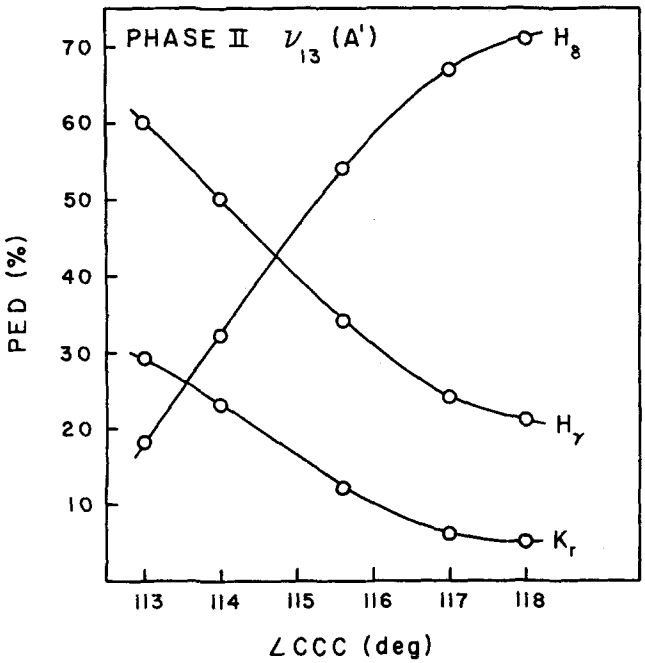

FIG. 6. $(PED)_{ii}$ sensitivity of the $\nu_{13}(A')$ phase II mode to changes in CCC bond angles. The CH_2 and CF_2 bond angles were held constant at 109.5°, with $G = 60°$.

configurational parameters were varied by small amounts around the parameters, which were used for the force constant refinement calculations,[11] in order to study the effects on the calculated frequencies and the $(PED)_{ii}$. The geometric sensitivity of the phase III modes was studied by considering the geometric dependence of the component conformations (phases I and II). The range of angular parameters investigated includes the parameters used in the force field refinement[11] and the average angular parameters found for the phase III chain.[10]

Phase I

The geometric dependence of phase I was investigated by doing two sets of calculations. The first set was done on a chain for which the CH_2 and CF_2 bond angles were held fixed at 109.5°, and the CCC bond angles were varied from 110° to 120°. The second set of calculations was done on a chain for which the CCC bond angles were held fixed at 117.6°, and the CH_2 and CF_2 bond angles were varied concurrently from 102° to 108°.

The calculated frequencies of all the phase I modes varied linearly over the range of CCC and CH_2 and CF_2 bond angles investigated in the two series of calculations. Tables V and VI list the calculated frequencies and $(PED)_{ii}$ for the smallest and largest CCC and CH_2 and CF_2 angles used in each series of calculations. As can be seen from these tables, large frequency shifts do occur, the largest change being 59 cm^{-1} for $\nu_2(B1)$ over the 10° CCC bond angle change. There are two cases for which the ordering of modes, with respect to frequency, are inverted over the angular range studied. When the CCC bond angles are varied, the $\nu_4(A1)$ and $\nu_3(B1)$ modes are inverted while each mode maintains essentially the same $(PED)_{ii}$. When the CH_2 and CF_2 bond angles are varied, the $\nu_3(A1)$ and $\nu_3(B2)$ modes are inverted, but again each mode maintains essentially the same $(PED)_{ii}$.

The $\nu_3(A1)$ mode is the only mode for which a component of the $(PED)_{ii}$ varies by more than 10% over the angular range studied. When the CCC bond angles are varied, the $(PED)_{ii}$ contribution from K_r goes from 47% to 34% while the contribution from H_ω increases from 46% to 49%. This is an inversion of the primary component of the $(PED)_{ii}$ for the $\nu_3(A1)$ mode. All other modes in phase I maintain essentially the same $(PED)_{ii}$ (i.e., changes by less than 10%) over the angular range investigated.

Phase II

The geometric dependence of phase II was investigated by doing two sets of calculations. The first set was done on a $TGTG'$ chain for which the CH_2 and CF_2 bond angles were held fixed at 109.5° and the *gauche* angle taken as 60°. The CCC bond angles were varied from 113° to 118°. The second set of calculations was done on a $TGTG'$ chain for which the CCC bond angles were held fixed at 114.9° and the *gauche* angle taken as 51.5°. The CH_2 and CF_2 bond angles were varied concurrently from 100° to 106°.

The calculated frequencies of the phase II modes vary linearly over the range of CCC and CH_2 and CF_2 bond angles investigated, with some exceptions. The CH_2 wagging and bending modes vary nonlinearly when the CCC angles are varied. The out-of-phase symmetric and antisymmetric CF_2 stretching modes vary nonlinearly when the CH_2 and CF_2 angles are varied. Tables VII and VIII list the calculated frequencies and $(PED)_{ii}$

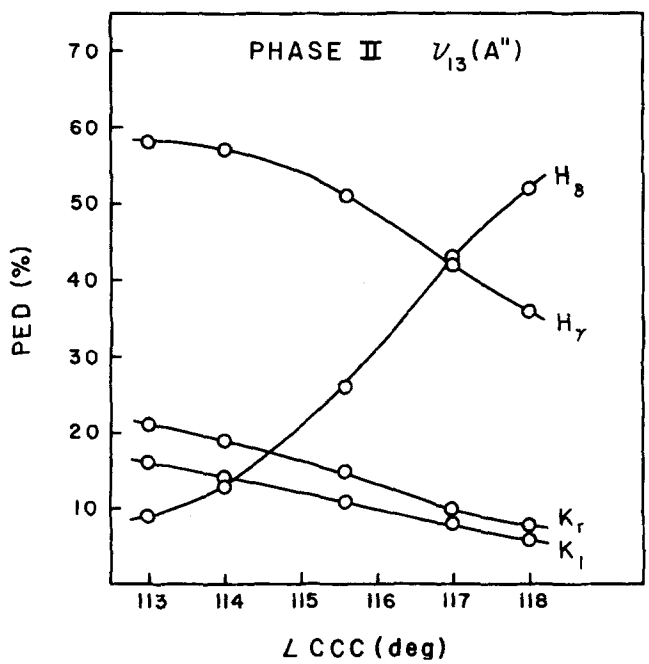

FIG. 7. $(PED)_{ii}$ sensitivity of the $\nu_{13}(A'')$ phase II mode to changes in CCC bond angles. The CH_2 and CF_2 bond angles were held constant at 109.5°, with $G = 60°$.

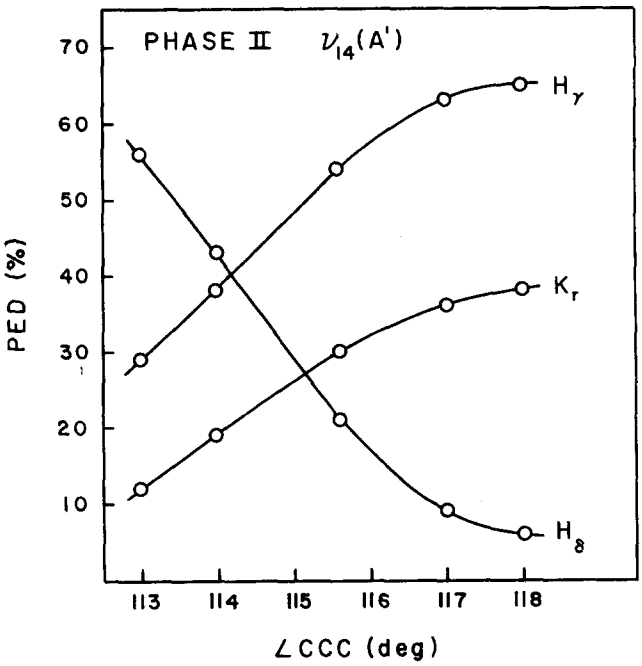

FIG. 8. $(PED)_{ii}$ sensitivity of the $\nu_{14}(A')$ phase II made to changes in CCC bond angles. The CH_2 and CF_2 bond angles were held constant at 109.5°, with $G = 60°$.

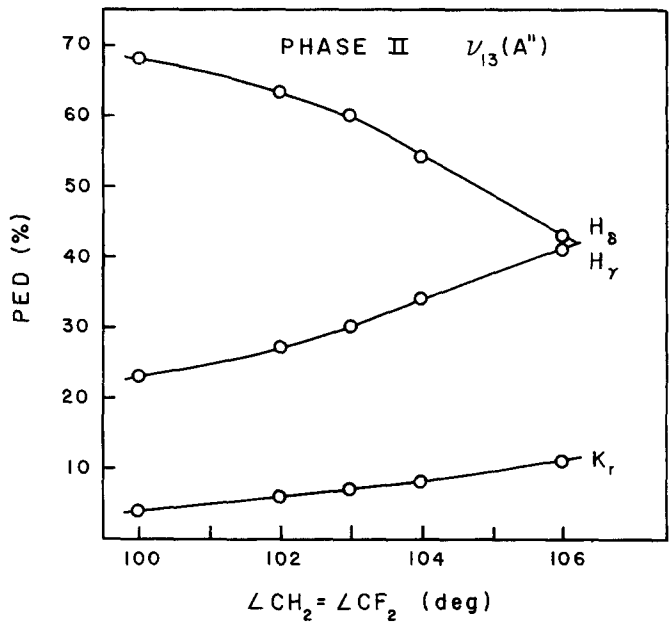

FIG. 10. $(PED)_{ii}$ sensitivity of the $\nu_{13}(A'')$ phase II mode to concurrent changes in CH_2 and CF_2 bond angles. The CCC bond angles were held constant at 114.9°, with $G = 51.5°$.

for the smallest and largest CCC and CH_2 and CF_2 angles used in the two sets of calculations.

There were two cases for which the ordering of modes with respect to frequency, are inverted over the angular ranges studied. When the CCC bond angles are varied, the $\nu_4(A')$ and $\nu_4(A'')$ modes are inverted. When the CH_2 and CF_2 bond angles are varied, the $\nu_5(A')$ and $\nu_5(A'')$ modes are inverted. In each case the $(PED)_{ii}$ remains essentially unchanged for each mode.

The phase II modes are much more susceptible to changes in the $(PED)_{ii}$ with angular changes than the phase I modes. When the CCC bond angles are varied, there are six modes for which the $(PED)_{ii}$ changes by at least 10%. Five of these modes experience an inversion of the primary component of the $(PED)_{ii}$ as a result of the geometry changes. These modes were $\nu_9(A')$, $\nu_{10}(A')$, $\nu_{13}(A')$, $\nu_{13}(A'')$, $\nu_{14}(A')$, and $\nu_{14}(A'')$. The most

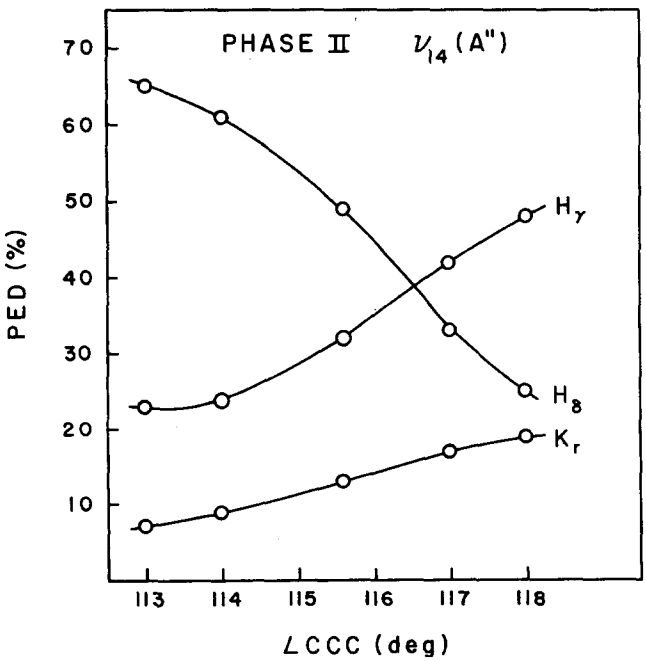

FIG. 9. $(PED)_{ii}$ sensitivity of the $\nu_{14}(A'')$ phase II mode to changes in CCC bond angles. The CH_2 and CF_2 bond angles were held constant at 109.5°, with $G = 60°$.

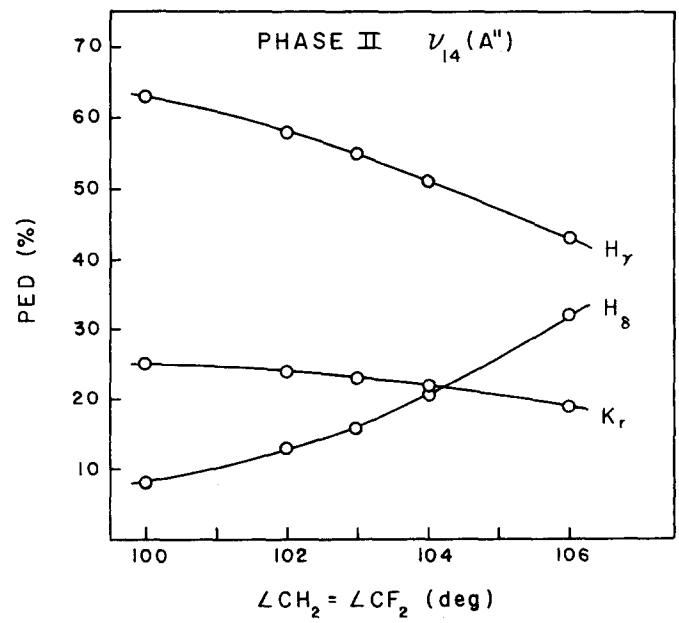

FIG. 11. $(PED)_{ii}$ sensitivity of the $\nu_{14}(A'')$ phase II mode to concurrent changes in CH_2 and CF_2 bond angles. The CCC bond angles were held constant at 114.9°, with $G = 51.5°$.

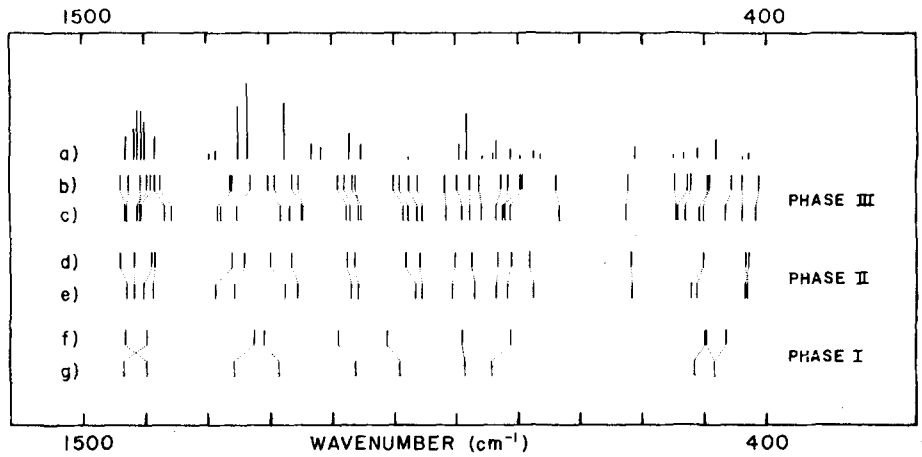

FIG. 12. (a) Representation of the observed phase III spectrum. (b) Calculated phase III spectrum: *TTT* segments with ∠CCC = 117.6°, ∠CH_2 and CF_2 = 105°; *TGT* segments with ∠CCC = 114.9°, ∠CH_2, and CF_2 = 103°, G = 51.5°. (c) Calculated phase III spectrum: *TTT* segments with ∠CCC = 113.1°, CH_2 and CF_2 = 109.5°; *TGT* segments with ∠CCC = 115.6°, ∠CH_2 and CF_2 = 109.5°, G = 60°. (d) Calculated phase II spectrum: ∠CCC = 114.9°, ∠CH_2 and CF_2 = 103°, G = 51.5°. (e) Calculated phase II spectrum: ∠CCC = 115.6°, ∠CH_2 and CF_2 = 109.5°, G = 60°. (f) Calculated phase I spectrum: CCC = 117.6°, CH_2 and CF_2 = 105°. (g) Calculated phase I spectrum: ∠CCC = 113.1°, ∠CH_2 and CF_2 = 109.5°.

dramatic of these $(PED)_{ii}$ changes occurs in the CH_2 wagging and bending modes. The variation of the $(PED)_{ii}$ of each component of these modes with respect to CCC bond angle is shown in Figs. 6 through 9.

When the CH_2 and CF_2 bond angles are varied, there are seven modes for which the $(PED)_{ii}$ changes by at least 10%. None of these seven modes experiences an inversion of the primary component of the $(PED)_{ii}$. Again, however, the CH_2 wagging and bending modes are the most sensitive to the geometry changes. The variation of the $(PED)_{ii}$ for each component of these modes [$\nu_{13}(A'')$ and $\nu_{14}(A'')$] with respect to CH_2 and CF_2 bond angle is shown in Figs. 10 and 11, respectively.

Some general trends of frequency shifts with geometry changes are common to both phase I and phase II. The frequency of the bands associated with the CH_2 and CF_2 twisting and wagging and CC stretching modes increases as the CCC bond angles are increased, and decreases as the CH_2 and CF_2 bond angles are increased. The frequency of the CH_2 and CF_2 rocking and bending modes decreases as the CCC bond angles are increased, and increases as the CH_2 and CF_2 bond angles are increased. The frequency of the symmetric CH_2 stretching mode remains essentially constant as the CCC bond angles increase, and decreases as the CH_2 and CF_2 bond angles increase. The frequency of the antisymmetric CH_2 stretching mode also remains essentially constant as the CCC bond angles are increased, and increases as the CH_2 and CF_2 bond angles increase.

Figure 12 diagrams the results of the frequency calculations of phases I, II, and III for the geometries employed in the force field refinement of Boerio and Koenig,[11] and the configurational parameters found for the *TTT* and *TGT*, *TG'T* segments in phase III, from crystal structure work.[10] As can be seen in Fig. 12, the modes of phase III shift in frequency with geometry changes in the same general fashion as do the corresponding phase I and phase II modes. As was the case for phase II, the $(PED)_{ii}$ of the CH_2 bending and wagging region of phase III is extremely sensitive to geometry changes. Several modes in this region involved inversions of the primary $(PED)_{ii}$ component.

CONCLUSIONS

A normal coordinate calculation was performed for an isolated chain having the conformation of phase III PVF_2. The agreement between the observed and calculated frequencies was good in that the fit for phase III was comparable to phases I and II. Excluding CH_2 stretching modes, the average percent error in phases I and II was 1.40%. Excluding the CH_2 stretching and CH_2 bending and wagging modes, the average percent error for phase III was 1.67%. The valence force field was refined[11] utilizing phase I and phase II data. The assumption that the valence force field could be transferred to phase III was valid.

With the exception of the CH_2 bending and wagging modes, approximate normal mode assignments were made for the phase III bands. The geometric sensitivity of both the calculated frequency and $(PED)_{ii}$ for some phase I and phase II modes has been demonstrated.

ACKNOWLEDGMENTS

Work was supported on NSF-MRL Grant to Case Western Reserve University under DMR78-24150. The authors acknowledge the assistance of Keith Gillis in the early stages of this work.

[1]J. B. Lando, H. G. Olf, and A. Peterlin, J. Polym. Sci. Part A 4, 941 (1966).
[2]R. Hasegawa, Y. Takahashi, Y. Chatani, and H. Tadokoro, Polym. J. 3, 600 (1972).
[3]W. W. Doll and J. B. Lando, J. Macromol. Sci. Phys. 4, 309 (1970).
[4]M. A. Bachmann and J. B. Lando, Macromolecules (in press).

[5]G. T. Davis, J. E. McKinney, M. G. Broadhurst, and S. C. Roth, J. Appl. Phys. **49**, 4998 (1978).
[6]G. R. Davies and H. Singh, Polymer **20**, 772 (1979).
[7]D. Naegele, D. Y. Yoon, and M. G. Broadhurst, Macromolecules **11**, 1297 (1978).
[8]M. A. Bachmann, W. L. Gordon, S. Weinhold, and J. B. Lando, J. Appl. Phys. **51**, 5095 (1980).
[9]S. Weinhold, M. H. Litt, and J. B. Lando, J. Polym. Sci. Polym. Lett. Ed. **17**, 585 (1979).
[10]S. Weinhold, M. H. Litt, and J. B. Lando, Macromolecules **13**, 1178 (1980).
[11]F. J. Boerio and J. L. Koenig, J. Polym. Sci. Part A **9**, 1517 (1971).
[12]M. Kobayashi, K. Tashiro, and M. Tadokoro, Macromolecules **8**, 158 (1975).
[13]F. J. Boerio and J. L. Koenig, J. Polym. Sci. Part A **7**, 1489 (1969).
[14]S. Enomoto, Y. Kawai, and M. Sugita, J. Polym. Sci. Part A **6**, 861 (1968).
[15]G. Cortili and G. Zerbi, Spectrochim. Acta Part A **23**, 285 (1967).
[16]M. A. Bachmann, W. L. Gordon, J. L. Koenig, and J. B. Lando, J. Appl. Phys. **50**, 6106 (1979).
[17]G. L. Cessac and J. G. Curro, J. Polym. Sci. Polym. Phys. Ed. **12**, 695 (1974).
[18]F. J. Boerio, Ph.D. Thesis, Case Western Reserve University (1971).
[19]M. J. Hannon, Ph.D. Thesis, Case Western Reserve University, (1969).
[20]R. G. Synder, J. Chem. Phys. **47**, 1316 (1967).
[21]F. J. Boerio and J. L. Koenig, J. Chem. Phys. **52**, 4826 (1970).
[22]G. Zerbi, Appl. Spectrosc. Rev. **2**, 193 (1969).
[23]C. G. Opaskar and S. Krimm, Spectrochim. Acta **21**, 1165 (1965).
[24]D. Lee, Spectrochim. Acta Part A **23**, 453 (1967).
[25]M. S. Wu, P. C. Painter, and M. M. Coleman, J. Polym. Sci. Polym. Phys. Ed. **18**, 111 (1980).
[26]M. S. Wu, P. C. Painter, and M. M. Coleman, J. Polym. Sci. Polym. Phys. Ed. **18**, 95 (1980).
[27]J. H. Schachtschneider and R. G. Snyder, Spectrochim. Acta **19**, 117 (1963).
[28]M. S. Wu, P. C. Painter, and M. M. Coleman, Spectrochim. Acta Part A **35**, 823 (1979).